

Micromagnetic study of the dipolar-exchange spin waves in antiferromagnetic thin films

Jiongjie Wang(王炯杰) and Jiang Xiao(肖江)

Citation: Chin. Phys. B, 2025, 34 (**10**): 107505. DOI: 10.1088/1674-1056/addaa4
http://cpb.iphy.ac.cn; http://iopscience.iop.org/cpb

What follows is a list of articles you may be interested in

Magnon behavior in YIG film under microwave excitation investigated by Brillouin light scattering

Guofu Xu(徐国服), Kang An(安康), Wenjun Ma(马文俊), Xiling Li(李喜玲), C. K. Ong, Chi Zhang(张驰), and Guozhi Chai(柴国志)
Chin. Phys. B, 2025, 34 (**6**): 067507. DOI: 10.1088/1674-1056/add24c

Orbital magnetic field effect on spin waves in a triangular lattice tetrahedral antiferromagnetic insulator

Pi-Ye Zhou(周丕烨), Xiao-Hui Li(李晓慧), and Yuan Wan(万源)
Chin. Phys. B, 2025, 34 (**6**): 067501. DOI: 10.1088/1674-1056/adca1f

Skyrmion motion induced by spin-waves on magnetic nanotubes

Tijjani Abdulrazak, Xuejuan Liu(刘雪娟), Zhenyu Wang(王振宇), Yunshan Cao(曹云姗), and Peng Yan(严鹏)
Chin. Phys. B, 2024, 33 (**10**): 107504. DOI: 10.1088/1674-1056/ad5d64

Tunable dispersion relations manipulated by strain in skyrmion-based magnonic crystals

Zhao-Nian Jin(金兆年), Xuan-Lin He(何宣霖), Chao Yu(于超), Henan Fang(方贺男), Lin Chen(陈琳), and Zhi-Kuo Tao(陶志阔)
Chin. Phys. B, 2024, 33 (**1**): 017501. DOI: 10.1088/1674-1056/acf03c

Magnonic band-pass and band-stop filters with structurally modulated waveguides

Lai-He Feng(冯来和), Mang-Yuan Ma(马莽原), Zhi-Hua Liu(刘智华), Kai-Le Xie(解凯乐), and Fu-Sheng Ma(马付胜)
Chin. Phys. B, 2023, 32 (**6**): 067503. DOI: 10.1088/1674-1056/ac8afb

---

SPECIAL TOPIC — Advanced magnonics

Micromagnetic study of the dipolar-exchange spin waves in antiferromagnetic thin films

Jiongjie Wang(王炯杰)[1] and Jiang Xiao(肖江)[1,2,3,4,†]

[1] *Department of Physics and State Key Laboratory of Surface Physics, Fudan University, Shanghai* 200433, *China*
[2] *Institute for Nanoelectronics Devices and Quantum Computing, Fudan University, Shanghai* 200433, *China*
[3] *Shanghai Research Center for Quantum Sciences, Shanghai* 201315, *China*
[4] *Hefei National Laboratory, Hefei* 230088, *China*

(Received 28 March 2025; revised manuscript received 19 May 2025; accepted manuscript online 20 May 2025)

In antiferromagnets, dipolar coupling is often disregarded due to the cancellation of magnetic moments between the two sublattices, so that the spin-wave dispersion is predominantly determined by exchange interactions. However, antiferromagnetic spin waves typically involve a slight misalignment of the magnetic moments on the sublattices, which gives rise to a small net magnetization enabling long-range dipolar coupling. In this paper, we investigate the role of dipolar coupling in spin-wave excitations and its influence on the resulting dispersion. Our findings show that: (i) when the Néel vector is perpendicular to the film plane or lies within the film plane and parallel to the wave vector, the dispersion branches can be divided into two groups: those unaffected by the dipolar field and those influenced by it. In these cases, the total magnetic moment remains linearly polarized, but the polarization directions differ between the two types of branches; (ii) when the Néel vector lies in the film plane and is perpendicular to the wave vector, the dipolar interactions affect both types of dispersion branches, leading to their hybridization. This hybridization alters the polarization of the magnetic moment, resulting in elliptical polarization.

Keywords: spin waves, spintronics, antiferromagnetics, magnetic properties of thin films

PACS: 75.30.Ds, 85.75.–d, 75.50.Ee, 75.70.–i

DOI: 10.1088/1674-1056/addaa4 **CSTR:** 32038.14.CPB.addaa4

1. Introduction

Spin waves,[1,2] the collective excitations of localized magnetic moments in ordered spin systems, have garnered significant attention for their fundamental importance and potential applications. In both ferromagnetic and antiferromagnetic (AFM) materials, these magnonic excitations propagate through the medium without involving net charge transport, thereby offering unique opportunities for low-power, highly efficient information processing in spintronic and magnonic devices.[3,4] Spin waves in ferromagnets and antiferromagnets exhibit distinctive dispersion relations and dynamics due to differences in their magnetic exchange interactions and symmetry properties, enabling a rich spectrum of physical phenomena that arise from their interaction with external fields, coupling to other quasiparticles, or structural inhomogeneities.

Spin waves in ferromagnetic materials can generally be classified into two types: exchange spin waves and dipolar spin waves.[1,2] Exchange spin waves dominate at short wavelengths and are governed by the strong quantum mechanical exchange interaction between neighboring spins. Dipolar spin waves, on the other hand, are prominent at longer wavelengths and are primarily influenced by the long-range dipolar interactions between magnetic moments. The comprehensive theory of dipolar-exchange spin waves in ferromagnetic thin films has been well established by De Wames *et al.*[5] and many others.[6–11]

Spin waves in antiferromagnetic materials are predominantly governed by exchange interactions due to the alternating alignment of magnetic moments within the lattice,[12–25] which cancels the net magnetization at the macroscopic scale. Spin waves in antiferromagnets exhibit a richer spectrum compared to ferromagnetic systems due to the presence of two spin sublattices, often leading to both acoustic and optical modes in their dispersion relations, as well as an additional polarization degree of freedom[26–29] that is absent in ferromagnetic spin waves. Dipolar spin waves are relatively less studied in antiferromagnetic materials because of the inherent cancellation of net magnetization, which minimizes the influence of long-range dipolar interactions. However, such cancellation does not hold when antiferromagnetic excitations occur, as a small net magnetization then arises, giving rise to dipolar coupling.

Micromagnetic simulations[30] have become a cornerstone in the study of spin waves within magnetic materials, offering deep insights into their dynamics and interactions. While simulations for ferromagnetic spin waves are well established due to the simpler single-sublattice dynamics and

[†]Corresponding author. E-mail: xiaojiang@fudan.edu.cn

© 2025 Chinese Physical Society and IOP Publishing Ltd. All rights, including for text and data mining, AI training, and similar technologies, are reserved.

their widespread applicability in magnonic devices, micromagnetic simulations for antiferromagnetic spin waves remain comparatively underdeveloped. This is largely attributed to the intrinsic challenges posed by their dual-sublattice structure and ultrafast precession frequencies, which demand advanced computational techniques. Nevertheless, recent innovations in numerical methods and the adaptation of simulation frameworks, such as COMSOL Multiphysics,[31] have made significant strides in overcoming these limitations. Specifically, the development of the `ms-comsol` module[32] in COMSOL Multiphysics facilitates the exploration of dipolar-exchange spin waves in antiferromagnetic systems.

In this paper, we present a new approach to simulating dipolar-exchange spin waves in antiferromagnetic thin films. We demonstrate the efficacy of combining the `ms-comsol` module, used for micromagnetic simulations, with the `mfnc` module, responsible for accurate calculation of dipolar fields. This combined methodology allows for a comprehensive simulation that captures the intricate interplay of dipolar and exchange interactions in these systems. We also analyze the dipolar-exchange spin waves in antiferromagnetic thin films and find that the dipolar field affects the spin-wave dispersions depending on their polarization states in the antiferromagnetic thin film. Our results provide valuable insights into the dynamic behavior, especially the polarization, of spin waves in antiferromagnetic materials, offering a foundation for future research in magnonics and spintronics.

2. Micromagnetic simulation of antiferromagnetic spin wave

Antiferromagnetic spin waves can be described by two coupled Landau–Lifshitz–Gilbert (LLG) equations[12]

$$\dot{\boldsymbol{m}}_1(\boldsymbol{r},t) = -\gamma \boldsymbol{m}_1 \times (\boldsymbol{H}_1 + \boldsymbol{h}) + \alpha \boldsymbol{m}_1 \times \dot{\boldsymbol{m}}_1, \quad \text{(1a)}$$

$$\dot{\boldsymbol{m}}_2(\boldsymbol{r},t) = -\gamma \boldsymbol{m}_2 \times (\boldsymbol{H}_2 + \boldsymbol{h}) + \alpha \boldsymbol{m}_2 \times \dot{\boldsymbol{m}}_2, \quad \text{(1b)}$$

where $\boldsymbol{H}_i = -\delta F(\boldsymbol{m}_1, \boldsymbol{m}_2)/\delta \boldsymbol{m}_i$ is the effective field acting on sublattice i with the free energy functional[4]

$$F(\boldsymbol{m}_1, \boldsymbol{m}_2) = \sum_i \int \mathrm{d}^3\boldsymbol{r}(f_i^{\mathrm{Z}} + f_i^{\mathrm{A}} + f_i^{\mathrm{E}}) + \int \mathrm{d}^3\boldsymbol{r} f^{\mathrm{E}}, \quad (2)$$

where $f_i^{Z,A,E}$ are the Zeeman, anisotropy, and intra-sublattice exchange energy densities for sublattice i, and f^{E} is the inter-sublattice exchange energy density between the two sublattices

$$f_i^{\mathrm{Z}} = -\mu_0 M_{\mathrm{s}} \boldsymbol{m}_i \cdot (\boldsymbol{H}_{\mathrm{ext}} + \boldsymbol{h}),$$

$$f_i^{\mathrm{A}} = -\frac{K}{2}(\boldsymbol{m}_i \cdot \hat{\boldsymbol{z}})^2,$$

$$f_i^{\mathrm{E}} = \frac{1}{2}A'(\nabla \boldsymbol{m}_i)^2,$$

$$f^{\mathrm{E}} = J\boldsymbol{m}_1 \cdot \boldsymbol{m}_2 - A(\nabla \boldsymbol{m}_1) \cdot (\nabla \boldsymbol{m}_2).$$

Here, the easy uniaxial anisotropy is along $\hat{\boldsymbol{z}}$ with strength K, so the equilibrium magnetic moments and the Néel vector are assumed to point along the $\hat{\boldsymbol{z}}$ direction. $A = Ja^2/2$ and $A' = J'a^2/2$ represent the inter- and intra-sublattice exchange couplings (Appendix A). The dipolar field $\boldsymbol{h} = \boldsymbol{h}(\boldsymbol{m})$ arises from the net magnetic moment distribution $\boldsymbol{m} = \boldsymbol{m}_1 + \boldsymbol{m}_2$. Two assumptions are made regarding the dipolar fields: (i) they are generated by the net moment $\boldsymbol{m}$, and the difference between the dipolar fields produced by $\boldsymbol{m}_1$ and $\boldsymbol{m}_2$ is neglected due to their atomic-scale separation; (ii) the dipolar fields acting on both sublattices are considered identical for the same reason.

By recombining the two sublattices into a net magnetic moment $\boldsymbol{m} = \boldsymbol{m}_1 + \boldsymbol{m}_2$ and a Néel vector $\boldsymbol{n} = \boldsymbol{m}_1 - \boldsymbol{m}_2$, we can rewrite Eq. (1) as the equivalent equations of motion for $\boldsymbol{m}$ and $\boldsymbol{n}$ (Eq. (B1) in Appendix B). When $J\boldsymbol{m}_1 \cdot \boldsymbol{m}_2$ is the dominant exchange coupling, which holds true for most natural antiferromagnets, the roles of the intralayer exchange A' and interlayer exchange A become interchangeable. To simplify the micromagnetic simulation, we use A' to represent both A and A', so that two independent LLG simulations for Eq. (1) can be coupled by exchanging only $\boldsymbol{m}_1$ and $\boldsymbol{m}_2$, without the need to communicate their gradients $\nabla \boldsymbol{m}_1$ and $\nabla \boldsymbol{m}_2$.

There are mainly three types of antiferromagnets (the A-type, C-type, and G-type[33,34]) as depicted in Fig. 1. For simplicity, we assume a cubic lattice with equal lattice constants in all three directions ($a = b = c$). If we consider only nearest-neighbor coupling and neglect next-nearest-neighbor coupling, the parametrizations for these three AFM types correspond to: (i) A-type, $\boldsymbol{A}' = A'(1,1,0)$, $\boldsymbol{A} = A(0,0,1)$; (ii) C-type, $\boldsymbol{A}' = A'(0,0,1)$, $\boldsymbol{A} = A(1,1,0)$; (iii) G-type, $\boldsymbol{A}' = 0$, $\boldsymbol{A} = A(1,1,1)$. In the following discussion, we focus on G-type antiferromagnets, where the exchange interaction remains isotropic.

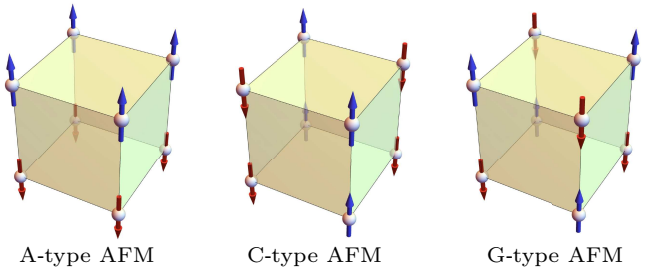


Fig. 1. Three types of antiferromagnets with a cubic lattice: A-type, C-type, and G-type.

In antiferromagnets, spin waves are predominantly governed by exchange interactions, and the dipolar fields are often neglected due to the near-complete cancellation of net magnetization arising from the two oppositely aligned sublattices. However, this cancellation breaks down in the presence of antiferromagnetic excitations, which induce a small but finite net magnetic moment, as first demonstrated by Keffer and

Kittel.[12] Consequently, these excitations give rise to nonvanishing dipolar fields that can influence the spin-wave dispersion.

We perform full micromagnetic simulations using the `ms-comsol` module — a micromagnetic simulation package we have developed on the COMSOL Multiphysics platform[31] over the past few years.[29,35–39] The module was originally designed for simulating ferromagnetic spin waves and was later extended to treat spin dynamics in synthetic antiferromagnets.[27] In this work, we further extend its capability to account for dipolar-field effects in antiferromagnetic spin waves. The simulations for antiferromagnets are implemented by treating the dynamics as two coupled ferromagnetic subsystems representing the two antiferromagnetic sublattices, based on Eq. (1), using the `ms-comsol` module.

The dipolar field is incorporated via the `mfnc` (magnetic fields, no current) module built into COMSOL, which solves the magnetic scalar potential in the quasi-static limit. The two modules are coupled self-consistently: the net magnetic moment

$$\boldsymbol{m}(\boldsymbol{r},t) = \boldsymbol{m}_1 + \boldsymbol{m}_2,$$

computed from the `ms-comsol` module, is passed to the `mfnc` module to determine the magnetic scalar potential and, consequently, the dipolar field $\boldsymbol{h}(\boldsymbol{r},t)$. The resulting dipolar field is then fed back into the `ms-comsol` module to update the magnetization dynamics. Through these iterative exchanges between the `ms-comsol` and `mfnc` modules, we achieve a fully self-consistent simulation of antiferromagnetic resonance, with dipolar interactions rigorously incorporated.

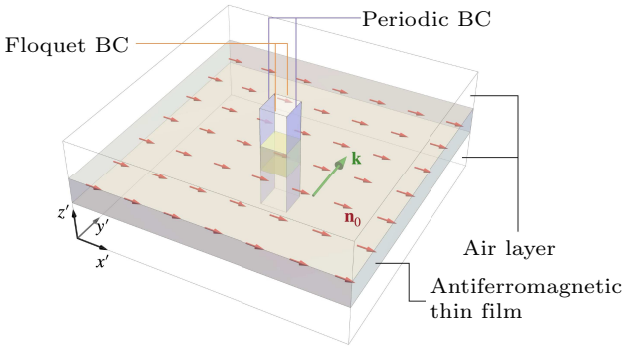


Fig. 2. Schematic diagram of the geometry and boundary conditions used in the micromagnetic simulation. The computational space includes the magnetic region for solving the LLG equation and the entire space for solving the magnetic Gauss's law. Due to the translational invariance of the infinitely large thin film, only a small pillar region needs to be simulated. Periodic boundary conditions are applied in the direction perpendicular to the wave vector, and Floquet boundary conditions are applied in the direction parallel to the wave vector. Here, x', y', z' denote the coordinate system of the thin film, with $\hat{z}'$ pointing along the film normal.

The system we focus on in this paper is an infinite antiferromagnetic thin film. To incorporate the dipolar fields in the `mfnc` module, we need to buffer the thin film with air layers above and beneath it (see Fig. 2). A periodic boundary condition is used along the direction perpendicular to the in-plane wavevector, and a Bloch–Floquet periodic boundary condition is used along the wavevector direction.[40] Consequently, only a one-dimensional strip along the thickness direction is required for simulation (the pillar region in Fig. 2), greatly reducing the simulation complexity and time. To further reduce the computational cost, we adopt the frequency-domain simulation for `comsol + mfnc` in COMSOL, which completely eliminates the need for temporal simulation. Details about the frequency-domain micromagnetic simulation using `ms-comsol` can be found in Ref. [39].

3. Semi-analytical approach

For the special case of infinite (anti-)ferromagnetic thin films considered in this paper, we can also employ a semi-analytical approach to calculate the spin wave dispersion. This method was developed by De Wames and Wolfram in the 1960s[5] for ferromagnets and was later applied to antiferromagnetic systems in the 1980s.[20]

The basic idea is to express the LLG equations in terms of the susceptibilities of $\boldsymbol{m}$ and $\boldsymbol{n}$ in response to the dipolar fields $\boldsymbol{h}$ in the frequency and reciprocal-space domains. On the other hand, the dipolar fields $\boldsymbol{h}$ and $\boldsymbol{m}$ satisfy Maxwell's equations under the quasi-static approximation. By expressing the dipolar fields in terms of an unknown magnetic scalar potential $\boldsymbol{h} = -\nabla\phi$, the coupled LLG and Maxwell equations can be reduced to a sixth-order ordinary differential equation for the scalar potential ϕ, based on the magnetic boundary conditions at the interfaces between the antiferromagnetic thin film and air. Eventually, the dispersion relation can be obtained by solving the eigenvalue problem associated with the sixth-order ordinary differential equation (see Appendix B for the detailed formulation).

The semi-analytical approach proves highly effective for homogeneous systems such as infinite thin films, making it a valuable tool for benchmarking micromagnetic simulations and examining dipolar-exchange spin-wave physics. However, its applicability diminishes when addressing nontrivial geometries or systems with inhomogeneous structures. In contrast, the micromagnetic simulations presented here offer greater flexibility and are well-suited for analyzing complex systems, including finite sizes, intricate geometries, and diverse magnetic textures.

4. Results

We now present the results of the dipolar-exchange antiferromagnetic spin-wave analysis. We first validate the `ms-comsol` simulation by comparing its results with those obtained from the semi-analytical approach. We then present the dispersions and spin-wave profiles for perpendicularly and in-plane magnetized antiferromagnetic thin films. The param-

eters used in the COMSOL simulation and semi-analytical calculation are summarized in Table 1.

Table 1. Parameters used in the calculation.[27,41]

Parameter	Value	Unit	Description
ω_{M}	34.5	GHz	saturation magnetization
K	$0.25\omega_{\mathrm{M}}$	GHz	anisotropy
J	$80\omega_{\mathrm{M}}$	GHz	inter-sublattice exchange
A	4.74×10^{-3}	GHz·μm^2	inter-sublattice exchange
A'	0	GHz·μm^2	intra-sublattice exchange
d	3.05	μm	film thickness
d_{air}	35.075	μm	upper/lower air thickness

We examine two distinct configurations regarding the orientation of the Néel vector relative to the film plane: (i) the perpendicular case, where the Néel vector is perpendicular to the film plane (i.e., $\boldsymbol{n}_0 \parallel \hat{\boldsymbol{z}} = \hat{\boldsymbol{z}}'$), and (ii) the in-plane case, where the Néel vector lies within the film plane. In the first scenario, the structure exhibits rotational symmetry about the $\hat{\boldsymbol{z}}$ axis, leading to a dispersion relation that depends only on the magnitude of the in-plane wave vector and is independent of its orientation. Conversely, in case (ii), the absence of rotational symmetry about the film normal leads to a dispersion relation that depends on both the magnitude and direction of the in-plane wave vector, characterized by the angle θ between $\boldsymbol{n}_0$ and $\boldsymbol{q}$.

4.1. Validation of `ms-comsol` simulation with dipolar fields

Figure 3 presents the dispersion relations obtained by micromagnetic simulation using the `ms-comsol` module (green crosses) and the semi-analytical approach (the grayscale color map) for the perpendicular and in-plane scenarios. The grayscale color map additionally illustrates the determinant of the M matrix in Appendix B, $-\sqrt{-\log|M(\omega,\boldsymbol{q})|}$, where local minima correspond to conditions under which the determinant vanishes, thereby indicating the eigenfrequencies of the spin-wave excitations. The green crosses represent the results from the `ms-comsol` module using the eigenvalue solver in COMSOL Multiphysics. The results are in excellent agreement, confirming the reliability of the `ms-comsol` simulation.

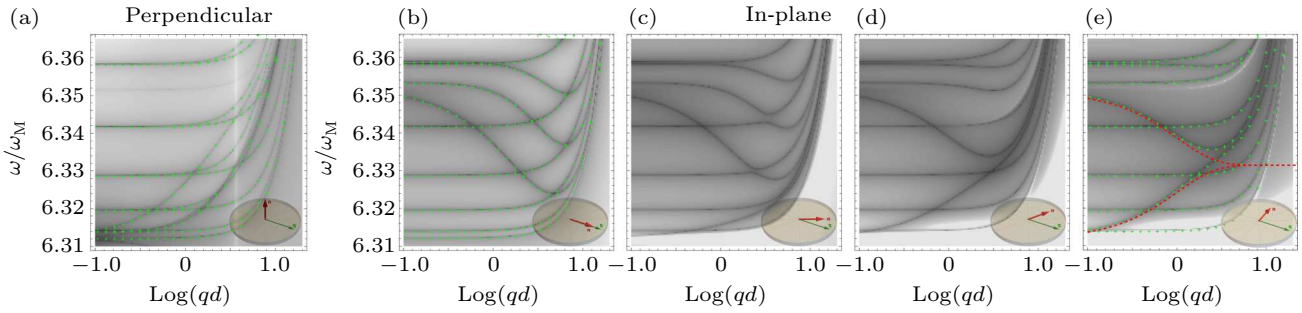


Fig. 3. Results from the semi-analytical calculation (gray-scale) and ms-comsol simulations (green crosses) for the perpendicular (a) and in-plane (b)–(e) magnetized thin film. The red and green arrows denote the directions of the Néel vector and the wave vector, respectively. For the in-plane case, the angles between the two vectors are $0, \pi/6, \pi/3$, and $\pi/2$, respectively. The red curves in the rightmost panel correspond to the dispersions of the dipolar spin surface wave modes in the long-wavelength limit (given by Eq. (C4) in Appendix C).

4.2. Dispersions and profiles

We now analyze the antiferromagnetic spin waves in detail by examining their dispersion relations and corresponding spin-wave profiles. Since the results from the semi-analytical approach and the COMSOL simulations are in excellent agreement as demonstrated in Fig. 3, we only present the results obtained from the COMSOL simulation using the `ms-comsol` + `mfnc` modules. Figure 4 shows detailed dispersions and corresponding spin-wave profiles for the perpendicular case and the in-plane case (for $\theta = 0$ and $\pi/2$).

To characterize the polarization of spin-wave excitations, we decompose the net magnetization ($\boldsymbol{m} = \boldsymbol{m}_1 + \boldsymbol{m}_2$) into three components based on their oscillation directions relative to the wave vector $\boldsymbol{q}$. This yields two types of polarization analogous to phonon polarizations: one longitudinal polarization, where the magnetization oscillates along $\boldsymbol{q}$, and two transverse polarizations, where the magnetization oscillates perpendicular to $\boldsymbol{q}$. Since $\boldsymbol{q}$ lies within the film plane, the longitudinal polarization is confined to in-plane oscillations, while the two perpendicular directions correspond to in-plane and out-of-plane transverse polarizations. In antiferromagnetic systems, only two polarization states can coexist due to the constraint that the magnetization is perpendicular to the Néel vector $\boldsymbol{n}_0$, effectively eliminating one possible direction and leaving a pair of polarizations that depend on the orientation of $\boldsymbol{n}_0$.

Figure 4(a) shows the dispersion and typical spin-wave profiles for the perpendicular case ($\boldsymbol{n}_0 \parallel \hat{\boldsymbol{z}}'$). The blue and red components correspond to the net magnetization $\boldsymbol{m}$ projected onto the in-plane transverse direction ($\boldsymbol{m}\cdot\boldsymbol{e}_{\mathrm{T}}^{\mathrm{in}}$, see lower right panel) and the longitudinal direction ($\boldsymbol{m}\cdot\boldsymbol{e}_{\mathrm{L}}$), respectively. The profiles show that only one component is nonzero for each mode, indicating that all eigenmodes are linearly polarized, either in the in-plane transverse polariza-

tion ($n = 1,2,4,7,9,11$) or the longitudinal in-plane polarization ($n = 3,5,6,8,10,12$). To illustrate the effect of dipolar fields, we also calculate the pure exchange spin-wave dispersion (dashed blue curves) by turning off the `mfnc` module. The modes with in-plane transverse polarization match the exchange-only dispersions, indicating that dipolar interactions do not affect these modes. In contrast, the modes with in-plane longitudinal polarization deviate from the exchange-only dispersions, especially at large q ($qd \gtrsim 1$), demonstrating that the longitudinal polarization is influenced by dipolar fields.

This distinction between the two in-plane polarizations arises naturally. For an infinite thin film with uniform in-plane magnetization, no dipolar fields are generated, which is the case for in-plane transverse polarization ($\boldsymbol{e}_{\mathrm{T}}^{\mathrm{in}}$). However, for in-plane longitudinal polarization ($\boldsymbol{e}_{\mathrm{L}}$), the magnetization alternates along the $\boldsymbol{q}$ direction, generating non-zero dipolar fields that modify the dispersion.

Figures 4(b) and 4(c) show results for cases with the Néel vector lying in the film plane ($\boldsymbol{n}_0 \perp \hat{\boldsymbol{z}}'$) at $\theta = 0$ (parallel to $\boldsymbol{q}$) and $\theta = \pi/2$ (perpendicular to $\boldsymbol{q}$), respectively. For the parallel case ($\boldsymbol{n}_0 \parallel \boldsymbol{q}$), similar to the perpendicular case in Fig. 4(a), all dispersion branches can be categorized into two types: modes affected or unaffected by the dipolar interaction, reflecting the polarization character of each mode. Modes with in-plane transverse polarization ($n = 1,2,3,4,6,9$) do not generate dipolar fields, while modes with out-of-plane transverse polarization ($n = 5,7,8$) produce dipolar (demagnetization) fields, resulting in lifted dispersions. At finite q, the magnetization alternates along $\boldsymbol{q}$, weakening the dipolar fields and producing downward bending in the dispersions, analogous to backward volume modes in ferromagnetic thin films.[42]

When the wave vector is perpendicular to the in-plane Néel vector ($\boldsymbol{q} \perp \boldsymbol{n}_0$), shown in Fig. 4(c), all dispersions are influenced by dipolar effects. The polarization degrees of freedom are now along the longitudinal direction ($\boldsymbol{e}_{\mathrm{L}} \parallel \boldsymbol{q}$) and out-of-plane transverse direction ($\boldsymbol{e}_{\mathrm{T}}^{\mathrm{out}} \parallel \hat{\boldsymbol{z}}'$). Both polarizations produce dipolar fields, resulting in dispersions modified by dipolar interactions. Unlike the previous scenarios where modes are linearly polarized, the eigenmodes here exhibit spatially varying elliptical polarization with components in both the longitudinal and out-of-plane transverse directions. This indicates that the longitudinal and out-of-plane transverse modes are coupled via dipolar interactions, forming hybridized normal modes with complex spatially varying polarizations. Modes with significant out-of-plane transverse components ($n = 5,7,9$) experience strong dipolar effects even as $q \to 0$, consistent with the strong demagnetization fields from out-of-plane magnetization. Modes with primarily longitudinal features ($n = 1,2,4,6,8$) exhibit dipolar effects only at finite wave vectors ($qd \gtrsim 1$), similar to the case in Fig. 4(a). Notably, the longitudinal mode for $n = 3$ shows particularly strong dipolar effects, due to its nearly uniform magnetization across the film thickness, minimizing field cancellation between layers.

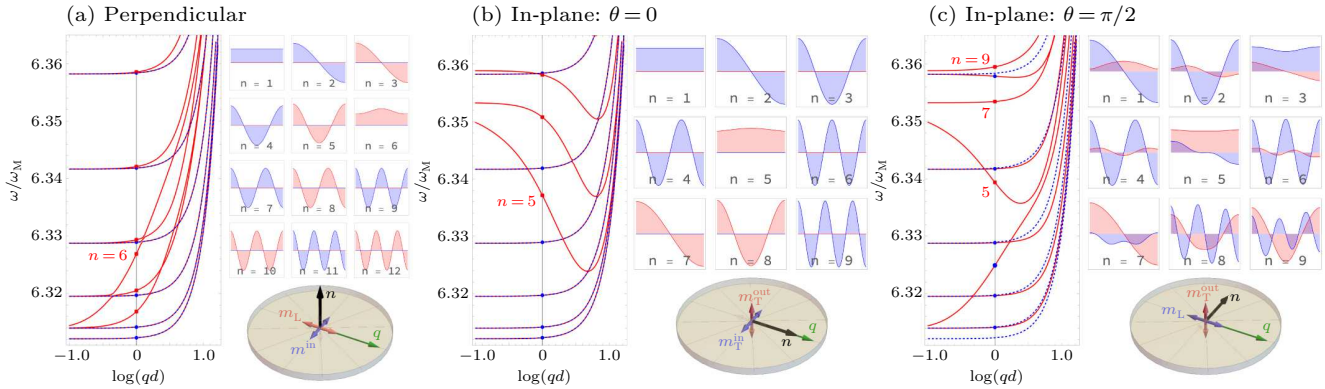


Fig. 4. Spin wave dispersion and spin wave profiles of the net magnetization for the perpendicularly magnetized (a) and in-plane magnetized (b, c) antiferromagnetic thin films. The blue and red components in the profiles correspond to the net magnetization $\boldsymbol{m}$ projected onto the two transverse directions indicated in the lower vector diagrams. Here, n denotes the branch index, ordered from low to high frequency.

5. Band structure of magnonic crystals

The semi-analytical approach, relying on plane-wave-like solutions, is inherently limited to handling homogeneous magnetization and idealized geometries, such as infinite thin films. In contrast, micromagnetic simulations using the `ms-comsol` module in COMSOL offer far greater flexibility, overcoming these constraints to model complex structures and inhomogeneous (anti-)ferromagnetic textures, with or without dipolar fields. One such scenario is the calculation of spin-wave band structures for magnonic crystals.

Traditionally, the calculation of spin-wave band structures in magnonic crystals typically requires large-scale spatial simulations and extended temporal evolution to obtain sufficient data for spatial and temporal Fourier transforms.[43–48] In contrast, by employing the `ms-comsol` method introduced in this paper, the simulation can be confined to a single unit cell in space by using the Floquet periodic boundary condition, similar to that used in built-in COMSOL modules such

as the electromagnetic waves, frequency domain (emw) module. Furthermore, the micromagnetic simulation can be carried out in the frequency domain,[39] thereby obviating the need for time-domain simulations. These simplifications in both spatial and temporal domains lead to significant reductions in computational time while achieving even higher accuracy in band-structure calculations.

We demonstrate the capability to calculate the spin-wave band structure of magnonic crystals using a simple example: a periodic array of circular antidots (holes) arranged in a square lattice in an antiferromagnetic thin film. We assume the Néel vector is perpendicular to the film plane, the radius of the circular holes (antidots) is $R = 0.4$ μm, spaced by a periodicity of $a = 1.8$ μm, as illustrated in Fig. 5(a). Other parameters are the same as those listed in Table 1.

Figure 5(b) shows the band structure along Γ–X–M–Γ in the Brillouin zone (inset of Fig. 5(a)) for the magnonic crystal calculated from `ms-comsol`. The band structure for the complete thin film without holes is shown as green curves in the background for comparison. At the boundary of the Brillouin zone, a band gap emerges due to scattering induced by the holes for the corresponding wavelength. Figure 5(c) shows the spatial distribution of the net magnetic moment modulus ($|\boldsymbol{m}_1 + \boldsymbol{m}_2|$) at points X_1, X_2, and M_1 in the dispersion curves. As the radius of the holes decreases to zero, these points continuously trace back to X_1', X_2', and M_1' on the dispersion for the thin film without holes.

Both X_1 and X_2 correspond to the first two standing-wave modes in the thickness direction but share the same in-plane wave vector $(k_x, k_y) = (2\pi/a, 0)$ along the x-direction. The intensity of X_1 is concentrated between the holes, while that of X_2 is concentrated along the holes. Additionally, X_1 has one node in the thickness direction, whereas X_2 has two nodes, confirming that they correspond to the first two standing-wave modes along the thickness. The M_1 mode has a wave vector $(k_x, k_y) = (2\pi/a, 2\pi/a)$.

Similar spin-wave band-structure calculations can be performed for a wide range of (anti-)ferromagnetic magnonic crystals, including systems with geometric structures, such as magnetic antidots or dots of arbitrary shapes and lattice arrangements, as well as those exhibiting inhomogeneous periodic magnetic textures, e.g., skyrmion crystals.

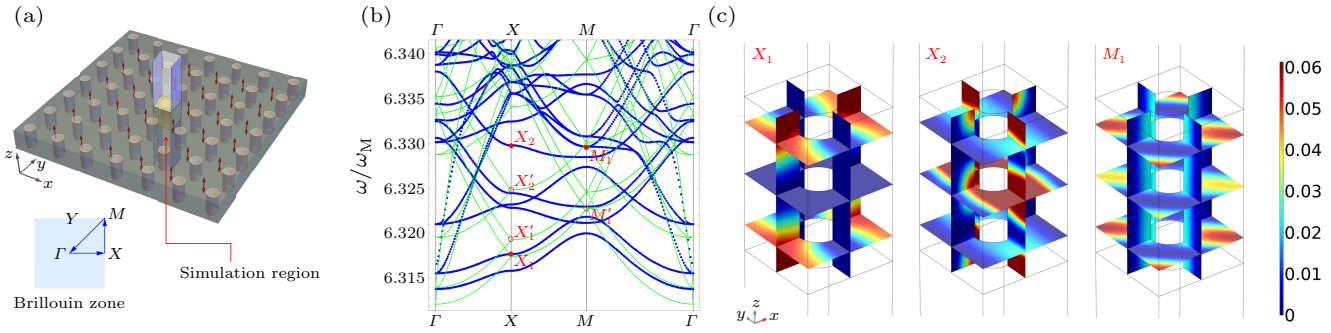


Fig. 5. (a) Real-space structure of antiferromagnetic magnonic crystals with antidots arranged in a cubic lattice. The equilibrium Néel vector is perpendicular to the thin film. (b) Band structure of the antidot array along the Γ–X–M–Γ path in the Brillouin zone. The background green lines represent the band structure of the complete thin film without holes for comparison. (c) Spatial distribution of the net magnetic moment within the unit cell corresponding to points X_1, X_2, and M_1 on the dispersion curve.

6. Discussion and conclusion

The polarization of antiferromagnetic spin waves is an intriguing topic. Here, we define polarization according to the net magnetic moment $\boldsymbol{m} = \boldsymbol{m}_1 + \boldsymbol{m}_2$, as illustrated in the profiles shown in Fig. 4. It can be seen from Fig. 4 that the antiferromagnetic spin wave eigenmodes are linearly polarized for the perpendicular case (where the Néel vector $\boldsymbol{n}$ is perpendicular to the film plane) and for the in-plane case with $\boldsymbol{q} \parallel \boldsymbol{n}$. In other configurations, the eigenmodes are not purely linearly polarized but exhibit non-trivial elliptical polarization with spatially dependent ellipticity. It is even possible that the spin wave is right-handed at one location and left-handed at another. Recent experimental techniques have been developed to detect the polarization of antiferromagnetic spin waves,[49] and varying spin-wave polarization has indeed been observed.

While our study focuses on dipolar spin waves in conventional antiferromagnetic materials, the approaches described in this paper also apply to antiferromagnetic van der Waals materials, which have attracted significant attention in recent years. Dipolar-exchange spin waves in these materials are expected to exhibit similar behaviors as in conventional antiferromagnets, albeit within a different range of material parameters. Most notably, because the intralayer and interlayer couplings differ significantly in van der Waals materials, the exchange interactions A and A' would be represented as vectors to account for direction-dependent coupling strengths.

In conclusion, our study affirms the validity of micromagnetic simulations for antiferromagnetic spin waves under the influence of dipolar fields, utilizing the `ms-comsol` module in COMSOL Multiphysics. By analyzing both disper-

sion relations and polarization characteristics, we identified distinct behaviors based on the orientation of the Néel vector. When the Néel vector is perpendicular to the film, the dispersion branches bifurcate into two linearly polarized categories: one with polarization parallel to the film and normal to the wavevector, remaining unaffected by dipolar fields, and another with polarization along the wavevector, which is influenced by dipolar fields for $qd > 1$. Conversely, when the Néel vector aligns with the wavevector, the branches again form two linearly polarized modes, with one remaining unaffected and parallel to the film, while the other exhibits film-perpendicular polarization influenced by dipolar fields even near $q \sim 0$. Interestingly, when the Néel vector lies parallel to the film but perpendicular to the wavevector, dipolar fields affect both polarization modes, leading to their hybridization into elliptically polarized waves. These findings enhance our understanding of antiferromagnetic spin-wave dynamics, particularly their interaction with dipolar fields under varying geometrical and material constraints.

Appendix A: Exchange coupling in AFM

The energy form of the lattice-regularized antiferromagnetic exchange interaction is

$$E_A = J_A \boldsymbol{S}_1 \cdot \boldsymbol{S}_2. \tag{A1}$$

When the spins of adjacent atoms are arranged in the opposite direction, the system is in a low-energy state. The dimension of J_A is $\mu_0 M_S^2 V$. Consider an alternating atomic structure: $a_0, b_0, a_1, b_1, a_2, b_2, a_3, b_3, \ldots$ For an atom on the a sublattice, the exchange interaction energy is

$$E_A = J_A \boldsymbol{S}_{ai} \cdot (\boldsymbol{S}_{b(i-1)} + \boldsymbol{S}_{bi}). \tag{A2}$$

The process of continuous approximation can be regarded as spreading the magnetic moments concentrated on the atoms over the unit cell. In this process, the dimensions of spatial volume and M_s are removed, resulting in a dimensionless $\boldsymbol{m}(x)$

$$\begin{aligned} e_A &= \frac{nJ_A}{(2a)^3} \boldsymbol{m}_a \cdot \left(2\boldsymbol{m}_b + a^2 \nabla^2 \boldsymbol{m}_b\right) \\ &= \frac{nJ_A}{4a^3} \boldsymbol{m}_a \cdot \boldsymbol{m}_b - \frac{nJ_A}{8a^3} a^2 \nabla \boldsymbol{m}_a \cdot \nabla \boldsymbol{m}_b. \end{aligned} \tag{A3}$$

The latter term is expanded in a Taylor series, where a is the unit cell edge length, and n is the number of atoms with antiferromagnetic interactions with a single atom. The parameters are concentrated into two terms: direct coupling between different lattices and exchange interaction

$$e_A = M_\mathrm{s}(J \boldsymbol{m}_a \cdot \boldsymbol{m}_b + A \boldsymbol{m}_a \cdot \nabla^2 \boldsymbol{m}_b), \tag{A4}$$

where

$$J = \frac{n_1 J_A}{4 M_\mathrm{s} a^3}, \quad A = \frac{n_1 J_A}{8 M_\mathrm{s} a}. \tag{A5}$$

Systems that can be described by the LLG equation in a continuous manner require that $a \ll \lambda$, where λ is the wavelength of the spin wave, i.e.,

$$\frac{A}{J} \ll \lambda^2 \sim \frac{1}{q^2 + q_x^2}, \tag{A6}$$

where q is the in-plane wave vector of the antiferromagnetic film, and q_x is the wave vector perpendicular to the film (with the film normal along the x direction).

Using the same approach, the expression for the ferromagnetic exchange interaction can be derived as

$$e_{\mathrm{F}i} = -\frac{1}{2} M_\mathrm{s} A' \boldsymbol{m}_i \cdot \nabla^2 \boldsymbol{m}_i \ \text{ with } \ A' = \frac{n_2 J_\mathrm{F}}{8 M_\mathrm{s} a'}, \tag{A7}$$

where a' is the distance within the same ferromagnetic lattice, J_F is the ferromagnetic exchange coupling, and n_2 is the number of atoms that have ferromagnetic exchange coupling with a specific atom. In order to match the form of antiferromagnetic exchange, we define

$$J' = \frac{n_2 J_\mathrm{F}}{4 M_\mathrm{s} a'^3}. \tag{A8}$$

Appendix B: Semi-analytical approach

For antiferromagnetic thin film with uniform Néel vector case, a semi-analytical approach is possible by mimicing the calculation of the dipolar-exchange spin wave for ferromagnetic thin film by De Wames and Wolfram,[50] and for antiferromagnet by Stamps and Camley.[20]

The coupled LLG equations Eq. (1) can be converted into the equations of motion for the Néel vector $\boldsymbol{n} = \boldsymbol{m}_1 - \boldsymbol{m}_2$ ($|\boldsymbol{n}| \simeq 2$) and net magnetization $\boldsymbol{m} = \boldsymbol{m}_1 + \boldsymbol{m}_2$ ($|\boldsymbol{m}| \ll 1, \boldsymbol{m} \cdot \boldsymbol{n} = 0$). Keeping up to the first order in small quantity of $\boldsymbol{m}, \boldsymbol{h}$ and neglecting the damping, Eq. (1) is rewritten as

$$\begin{aligned} \frac{\dot{\boldsymbol{n}}}{\gamma} &= -\boldsymbol{m} \times K\hat{\boldsymbol{z}} - \boldsymbol{n} \times (\boldsymbol{H}_\mathrm{ext} - J\boldsymbol{m} + \boldsymbol{h} - \frac{A - A'}{2} \nabla^2 \boldsymbol{m}) \\ &\simeq -\boldsymbol{m} \times K\hat{\boldsymbol{z}} - \boldsymbol{n} \times (\boldsymbol{H}_\mathrm{ext} - J\boldsymbol{m} + \boldsymbol{h}), \end{aligned} \tag{B1a}$$

$$\frac{\dot{\boldsymbol{m}}}{\gamma} = -\boldsymbol{m} \times \boldsymbol{H}_\mathrm{ext} - \boldsymbol{n} \times (K\hat{\boldsymbol{z}} + \frac{A + A'}{2} \nabla^2 \boldsymbol{n}). \tag{B1b}$$

The approximation in the equation for $\dot{\boldsymbol{n}}$ assumes that $J \gg (A - A')\nabla^2$, i.e., $J \gg (A - A')q^2$, thus the ∇^2 term in the $\dot{\boldsymbol{n}}$ equation can be neglected. With this approximation, A and A' only appear in the equation of motion (EOM) for $\dot{\boldsymbol{m}}$, and have exactly the same effect on the results, therefore there is no need to distinguish A, A'. In the simulation, we can replace the inter-lattice exchange interaction A with the exchange interaction A' within a single lattice. From Eq. (B1), one see that the dipolar field only enters the EOM for $\dot{\boldsymbol{n}}$. The effect of dipolar field on $\dot{\boldsymbol{m}}$ has the form of $\boldsymbol{m} \times \boldsymbol{h}(\boldsymbol{m})$, which is second order in $\boldsymbol{m}$, thus neglected in the linearized equation above.

We now consider the equilibrium magnetic moments of the two sublattices point in $\hat{\boldsymbol{z}}$: $\boldsymbol{m}_1^0 = \hat{\boldsymbol{z}}$, $\boldsymbol{m}_2^0 = -\hat{\boldsymbol{z}}$. And let $\boldsymbol{m}_\perp = (m_x, m_y)$, $\boldsymbol{n}_\perp = (n_x, n_y)$ be the small deviation due to excitation, and $\boldsymbol{h}_\perp = (h_x, h_y)$ is the resulting dipolar fields due to $\boldsymbol{m}_\perp$. Note that $\boldsymbol{m}_z \sim 0$, $\boldsymbol{n}_z \sim 2$, Eq. (B1) can be rewritten as a linear response equation

$$\boldsymbol{m}_\perp = \chi_m \gamma \boldsymbol{h}_\perp, \quad \boldsymbol{n}_\perp = \chi_n \gamma \boldsymbol{h}_\perp, \tag{B2}$$

where the magnetic and Néel susceptibility ($\omega_0 \equiv \gamma H_{\text{ext}}$)

$$\chi_m = \frac{2\hat{\Omega}}{\hat{W}^4 - 4\omega^2\omega_0^2} \begin{pmatrix} \hat{W}^2 & -2\mathrm{i}\omega\omega_0 \\ 2\mathrm{i}\omega\omega_0 & \hat{W}^2 \end{pmatrix} \xrightarrow{\omega_0=0} 2\hat{\Omega}\hat{W}^{-2}, \tag{B3a}$$

$$\chi_n = \begin{pmatrix} -\omega_0 & \mathrm{i}\omega \\ -\mathrm{i}\omega & -\omega_0 \end{pmatrix} \hat{\Omega}^{-1}\chi_m \xrightarrow{\omega_0=0} -\omega\sigma_y\hat{W}^{-2}, \tag{B3b}$$

where we defined two operators

$$\hat{W}^2 \equiv (K+2J)\hat{\Omega} - \omega^2 - \omega_0^2, \quad \hat{\Omega} \equiv K - (A+A')\nabla^2.$$

The second equal signs in Eq. (B3) applies in the absence of external field ($\omega_0 = 0$).

In quasistatic approximation, the dipolar magnetic field $\boldsymbol{h}(\boldsymbol{r},t)$ satisfies $\nabla \times \boldsymbol{h} = 0$, which means that the field can be represented by a scalar potential: $\boldsymbol{h}(\boldsymbol{r},t) = -\nabla\psi(\boldsymbol{r},t)$. The magnetic flux $\boldsymbol{b}(\boldsymbol{r},t)$ satisfy the Maxwell's equations in the quasistatic approximation

$$\nabla\cdot\boldsymbol{b} = \nabla\cdot(\boldsymbol{h} + \mu_0 M_s \boldsymbol{m}) = 0, \quad \text{inside the film}, \tag{B4a}$$

$$\nabla\cdot\boldsymbol{b} = \nabla\cdot\boldsymbol{h} = 0, \quad \text{outside the film}. \tag{B4b}$$

The transverse dipolar field is related to the full dipolar field as $\boldsymbol{h}_\perp = \boldsymbol{h} - \hat{\boldsymbol{z}}h_z = -\nabla\psi + \hat{\boldsymbol{z}}\partial_z\psi$. Equations (B2)–(B4) completely determine the properties of the dipolar-exchange spin waves in antiferromagnet.

The net magnetization $\boldsymbol{m}$ can be written in terms of the scalar potential ψ via $\boldsymbol{m} \simeq \boldsymbol{m}_\perp = \chi_m\gamma\boldsymbol{h}_\perp$, therefore the equations in Eq. (B4) can be also be expressed in terms of the scalar potential ($\omega_{\text{M}} \equiv \gamma M_s$)

$$\left[(\hat{W}^2 + 2\omega_{\text{M}}\hat{\Omega})\hat{W}^2 - 4\omega^2\omega_0^2\right]\nabla^2\psi = 2\omega_{\text{M}}\hat{\Omega}\hat{W}^2\partial_z^2\psi, \tag{B5a}$$

$$\nabla^2\psi = 0. \tag{B5b}$$

The equations above, equivalent to Eqs. (B2)–(B4), governs the full dynamical information about the dipolar fields and the magnetic moments of the antiferromagnetic thin film. Once the scalar potential ψ is solved using Eq. (B5), the dipolar field and the magnetic moment $\boldsymbol{m}(\boldsymbol{r},t)$ can be infered straightforwardly. Since both $\hat{W}^2$ and $\hat{\Omega}$ involve Laplacian operators, Eq. (B5) is a set of 6th-order ordinary differential equations. If restore the neglected term in Eq. (B1), the 6th-order becomes 10th-order. In comparison, the equivalent equation for ferromagnetic case is 6-th order.[50]

The EOM for $\psi(\boldsymbol{r},t)$ in Eq. (B5) can only be solved with proper boundary conditions at the interfaces between the antiferromagnetic thin film and the vacuum. We use another coordinates (x',y',z') with z' perpendicular to the thin film plane, and the two interfaces are at $z' = 0,\ d$. The easy axis $\hat{\boldsymbol{z}} = \hat{\boldsymbol{x}}'\sin\eta + \hat{\boldsymbol{z}}'\cos\eta$, or the film normal $\hat{\boldsymbol{z}}' = \hat{\boldsymbol{x}}\sin\eta + \hat{\boldsymbol{z}}\cos\eta$. The boundary conditions for the dipolar fields require the continuity of the following components across the interfaces

$$\hat{\boldsymbol{z}}'\times\boldsymbol{h}\big|_{z'=0,d}, \quad \hat{\boldsymbol{z}}'\cdot\boldsymbol{b}\big|_{z'=0,d}. \tag{B6}$$

In addition, by integrating the second equation of Eq. (B1) over a tiny distance across the interfaces, we find another set of boundary condition, i.e., zero flux for $\boldsymbol{n}$

$$\boldsymbol{n}\times\frac{\partial\boldsymbol{n}}{\partial z'}\bigg|_{z'=0,d} = 0. \tag{B7}$$

Let $\boldsymbol{u} = (x',y')$ and $\boldsymbol{k} = (k_{x'},k_{y'})$ be the in-plane position and wavevector, we use following ansatz solution in Eq. (B5)

$$\psi(\boldsymbol{r},t) = \begin{cases} \phi(0)\,\mathrm{e}^{+kz'}\,\mathrm{e}^{-\mathrm{i}\boldsymbol{k}\cdot\boldsymbol{u}}\,\mathrm{e}^{\mathrm{i}\omega t}, & z' < 0, \\ \phi(z')\,\mathrm{e}^{-\mathrm{i}\boldsymbol{k}\cdot\boldsymbol{u}}\,\mathrm{e}^{\mathrm{i}\omega t}, & 0 < z' < d, \\ \phi(d)\,\mathrm{e}^{-kz'}\,\mathrm{e}^{-\mathrm{i}\boldsymbol{k}\cdot\boldsymbol{u}}\,\mathrm{e}^{\mathrm{i}\omega t}, & z' > d. \end{cases} \tag{B8}$$

This ansatz enables the replacement of the Laplacian operator $\nabla^2 \to \partial_{z'}^2 - k^2$, and it automatically satisfies Eq. (B5b) as well as the boundary conditions for $\boldsymbol{h}$ in Eq. (B6). The remaining equation need to be solved is Eq. (B5a) with the zero-flux boundary condition Eq. (B7) and the boundary conditions for $\boldsymbol{b}$ in Eq. (B6). Equation (B5a) is a standard six-order ordinary differential equation of $\phi(z')$ in $\partial_{z'}$, which can be solved via the Euler method with six exponential solutions

$$\phi(z') = \sum_{j=1}^{6} c_j\,\mathrm{e}^{-\mathrm{i}q_j z'} = \sum_{j=1}^{3}(a_j\,\mathrm{e}^{\mathrm{i}q_j z'} + b_j\,\mathrm{e}^{-\mathrm{i}q_j z'}), \tag{B9}$$

where $\pm q_j$ are the six roots to the polynomial equation corresponding to the 6-th ordinary differential equation Eq. (B5a). The six exponential are rearranged into positive and negative pairs because Eq. (B5a) only contains the even order of $\partial_{z'}$. The six unknown coefficients a_j, b_j are determined by the six boundary conditions for $\boldsymbol{m}$ in Eq. (B6) and for zero-flux in Eq. (B7) at $z' = 0, d$

$$\partial_{z'}\phi + \sin\eta\,(\chi_m^{xx}\partial_x - \mathrm{i}\chi_m^{xy}k_y)\,\phi \mp k\phi = 0, \tag{B10a}$$

$$\partial_{z'}\chi_n \begin{pmatrix} \partial_x \\ -\mathrm{i}k_y \end{pmatrix}\phi = 0, \tag{B10b}$$

where $\partial_{z'} = \sin\eta\,\partial_x + \cos\eta\,\partial_z$, and $\pm k$ in the first equation corresponds to the two interfaces at $z' = 0, d$, respectively. By plugging Eq. (B9) in the equations above, Eq. (B10) becomes a set of linear equations with six unknowns

$$M(\eta,\omega,\boldsymbol{k})\begin{pmatrix} a_1 & b_1 & a_2 & b_2 & a_3 & b_3 \end{pmatrix}^{\mathrm{T}} = 0. \tag{B11}$$

The dispersion of the dipolar-exchange antiferromagnetic spin wave for a given in-plane wave-vector $\boldsymbol{k}$ is solved by finding the roots in ω that making the determinant of the coefficient matrix vanish

$$|M(\eta,\omega,\boldsymbol{k})| = 0. \tag{B12}$$

The corresponding spin wave profile is found by solving for the coefficients a_j, b_j in Eq. (B11) at the resonant frequencies.

Appendix C: Dipole surface spin waves in the long-wavelength limit

For the in-plane magnetized case ($\boldsymbol{n}_0 \perp \hat{\boldsymbol{z}}'$), when the in-plane wave vector is perpendicular to the in-plane Néel vector ($\boldsymbol{k} \perp \boldsymbol{n}_0$), the equation of motion for the magnetic scalar potential ψ in the long wavelength limit ($qd \ll 1$) is

$$\left[\left(\hat{W}^2 + 2\omega_{\mathrm{M}}K\right)\hat{W}^2 - 4\omega^2\omega_0^2\right]\left(k^2 + q_j^2\right)\psi = 0, \tag{C1}$$

which is solved by

$$k^2 + q_j^2 = 0 \Rightarrow q_j = \pm \mathrm{i}k. \tag{C2}$$

This solution corresponds to a surface spin wave. By substituting $q_j = \pm \mathrm{i}k$ into the boundary condition given by Eq. (B10)

$$\left(1 + \frac{2\omega_{\mathrm{M}}K\hat{W}^2}{\hat{W}^4 - 4\omega^2\omega_0^2}\right)\partial_x\phi + \frac{4\omega\omega_0\omega_{\mathrm{M}}K}{\hat{W}^4 - 4\omega^2\omega_0^2}k\phi \mp k\phi = 0, \tag{C3}$$

we have the dispersion for the surface spin wave

$$\begin{aligned}\omega^2 \;=\; & K(K + 2J + \omega_{\mathrm{M}}) + \omega_0^2 \\ & \pm\sqrt{4K(K + 2J + \omega_{\mathrm{M}})\omega_0^2 + \omega_{\mathrm{M}}^2K^2\,\mathrm{e}^{-2kd}}.\end{aligned} \tag{C4}$$

They are the analytical expressions for the lowest-order modes of the two dispersion branches in Fig. 4(c) when $qd \ll 1$, exhibiting surface wave characteristics. In these two modes, the excitation strengths of the magnetic moments of the two sublattices are concentrated on the upper and lower surfaces, respectively. However, the total magnetic moment does not possess surface wave characteristics. Only when an external magnetic field is applied can a distinct surface wave characteristic be observed in the net magnetic moment.

Acknowledgments

This project was supported by the National Natural Science Foundation of China (Grant No. 12474110), the National Key Research and Development Program of China (Grant No. 2022YFA1403300), the Innovation Program for Quantum Science and Technology (Grant No. 2024ZD0300103), and the Shanghai Municipal Science and Technology Major Project (Grant No. 2019SHZDZX01).

References

[1] Gurevich A G and Melkov G A 1996 *Magnetization Oscillations and Waves* (Boca Raton: CRC Press)
[2] Stancil D D and Prabhakar A 2009 *Spin Waves* (New York: Springer)
[3] Chumak A V, Vasyuchka V I, Serga A A and Hillebrands B 2015 *Nat. Phys.* **11** 453
[4] Yu H, Xiao J and Schultheiss H 2021 *Phys. Rep.* **905** 1
[5] De Wames R E and Wolfram T 1969 *Phys. Rev.* **185** 752
[6] Goedsche F 1970 *Phys. Status Solidi B* **41** 711
[7] Kalinikos B A 1981 *Sov. Phys. J.* **24** 718
[8] Mika K and Grünberg P 1985 *Phys. Rev. B* **31** 4465
[9] Kalinikos B A and Slavin A N 1986 *J. Phys. C: Solid State Phys.* **19** 7013
[10] Hillebrands B 1990 *Phys. Rev. B* **41** 530
[11] Harms J S and Duine R A 2022 *J. Magn. Magn. Mater.* **557** 169426
[12] Keffer F and Kittel C 1952 *Phys. Rev.* **85** 329
[13] Marshall W 1955 *Proc. R. Soc. Lond. A* **232** 69
[14] Oguchi T 1960 *Phys. Rev.* **117** 117
[15] des Cloizeaux J and Pearson J J 1962 *Phys. Rev.* **128** 2131
[16] Loudon R and Pincus P 1963 *Phys. Rev.* **132** 673
[17] Wolfram T and De Wames R E 1969 *Phys. Rev.* **185** 762
[18] Camley R E 1980 *Phys. Rev. Lett.* **45** 283
[19] Lüthi B and Hock R 1983 *J. Magn. Magn. Mater.* **38** 264
[20] Stamps R L and Camley R E 1987 *Phys. Rev. B* **35** 1919
[21] Pereira J M and Cottam M G 1999 *J. Appl. Phys.* **85** 4949
[22] Wieser R, Vedmedenko E Y and Wiesendanger R 2009 *Phys. Rev. B* **79** 144412
[23] Shen K 2020 *Phys. Rev. Lett.* **124** 077201
[24] Liu J, Wang L and Shen K 2020 *Phys. Rev. Res.* **2** 023282
[25] Sun Y, Meng F, Lee C, Soll A, Zhang H, Ramesh R, Yao J, Sofer Z and Orenstein J 2024 *Nat. Phys.* **20** 794
[26] Cheng R, Daniels M W, Zhu J G and Xiao D 2016 *Sci. Rep.* **6** 24223
[27] Lan J, Yu W and Xiao J 2017 *Nat. Commun.* **8** 178
[28] Proskurin I, Stamps R L, Ovchinnikov A S and Kishine J i 2017 *Phys. Rev. Lett.* **119** 177202
[29] Yu W, Lan J and Xiao J 2018 *Phys. Rev. B* **98** 144422
[30] Abert C 2019 *Eur. Phys. J. B* **92** 120
[31] Comsol A B *COMSOL Multiphysics*
[32] Yu W *COMSOL Blog: Micromagnetic Simulation with COMSOL Multiphysics*
[33] Solovyev I V 1997 *Phys. Rev. B* **55** 8060
[34] Treves D 1962 *Phys. Rev.* **125** 1843
[35] Lan J, Yu W, Wu R and Xiao J 2015 *Phys. Rev. X* **5** 041049
[36] Yu W, Lan J, Wu R and Xiao J 2016 *Phys. Rev. B* **94** 140410
[37] Yu W, Lan J and Xiao J 2020 *Phys. Rev. Appl.* **13** 024055
[38] Yu W, Xiao J and Bauer G E W 2021 *Phys. Rev. B* **104** L180405
[39] Zhang J, Yu W, Chen X and Xiao J 2023 *AIP Adv.* **13** 055108
[40] van den Boom S J, van Keulen F and Aragon A M 2021 *Comput. Methods Appl. Mech. Eng.* **382** 113848
[41] Yan P, Wang X S and Wang X R 2011 *Phys. Rev. Lett.* **107** 177207
[42] Prabhakar A and Stancil D D 2009 *Spin Waves: Theory and Applications* (Boston: Springer)
[43] Dvornik M and Kruglyak V V 2011 *Phys. Rev. B* **84** 140405
[44] Kumar D, Dmytriiev O, Ponraj S and Barman A 2011 *J. Phys. D: Appl. Phys.* **45** 015001
[45] Schwarze T, Huber R, Duerr G and Grundler D 2012 *Phys. Rev. B* **85** 134448
[46] Han D S, Vogel A, Jung H, Lee K S, Weigander M, Stoll H, Schütz G, Fischer P, Meier G and Kim S K 2013 *Sci. Rep.* **3** 2262
[47] Krawczyk M and Grundler D 2014 *J. Phys.: Condens. Matter* **26** 123202
[48] Qin H, Both G J, Hämäläinen S J, Yao L and van Dijken S 2018 *Nat. Commun.* **9** 5445
[49] Sheng L, Duvakina A, Wang H, Yamamoto K, Yuan R, Wang J, Chen P, He W, Yu K, Zhang Y, Chen J, Hu J, Song W, Liu S, Han X, Yu D, Ansermet J P, Maekawa S, Grundler D and Yu H 2025 *Nat. Phys.* **21** 740
[50] De Wames R E and Wolfram T 1970 *J. Appl. Phys.* **41** 987